Available online at www.sciencedirect.com
ScienceDirect
International Journal of Mass Spectrometry 263 (2007) 298–303
International Journal of Mass Spectrometry
www.elsevier.com/locate/ijms

Prompt in situ emission of gold adducts from single impacts of large gold clusters on organics solids

C. Guillermier [a], S. Della Negra [b], R.D. Rickman [a], G.J. Hager [a], E.A. Schweikert [a,*]

[a] *Department of Chemistry, Texas A&M University, College Station, TX 77842-3012, USA*
[b] *Institut de Physique Nucléaire d'Orsay, CNRS-IN2P3, 91406 Orsay, France*

Received 7 November 2006; received in revised form 16 March 2007; accepted 16 March 2007
Available online 25 March 2007

Abstract

We report the first observation of single impacts of 136 keV Au_n^{4+} ($100 \leq n \leq 400$) on organic solids, generating prolific emission of Au and Au_2 - containing fragments and molecular ions. We show that the individual impacting cluster is both the source of energy stimulating the emission, and the donor of atoms for adducts synthesis. The emission of Au and Au_2 was observed when $n \geq 100$. The most abundant species is $Au(CN)_2^-$. The adduct yields behave as follows when the projectile size varies from $n = 100$ to 400: (a) they increase with n; (b) the dependence with n for the formation of $Au(CN)_2^-$ differs from those for more complex species suggesting different pathways of synthesis; (c) the combined yields of the Au or the Au_2 - adducts are the same for different targets. There is evidence that the projectiles were implanted virtually intact in the organic targets, thus, the adduct synthesis involves a small number of Au atoms ablated from the projectile, which implies extensive ionization of the detached atoms. The abundance of three-body assemblies, e.g. $Au(CN)_2^-$, Au(CN) $(M–H)^-$, suggests that the adduct formation occurs likely in a dense phase.

Keywords: Au-adduct formation; Cluster–solid interaction; Re-emission of projectile atoms; Extreme chemistry

1. Introduction

It was shown some years ago that bombardment with polyatomic projectiles results in a non-linear enhancement of the secondary ion (SI) emission, specifically the emission of cluster and molecular ions [1,2]. For example, the SI yields obtained with Au_3^+–Au_5^+ projectiles are at least 10 times higher than those obtained with Au^+. This comparison is for projectiles at equal velocities in the range of 5–60 keV. Recent work with Bi_n^+ ($1 \leq n \leq 7$) shows similar trends for the SI emission [3]. Experiments with more complex projectiles, in particular C_{60}^+, demonstrate that the SI yield enhancement is correlated with the energy deposited in the very near surface region (<10 nm). Experimental work [4] and molecular dynamics (MD) simulations [5,6] indicate that, at equal impact energy, C_{60}^+ is more efficient in generating ionized ejecta than Au_3^+. Thus, the energy density is the main parameter of the SI emission. One way to further increase the energy density is to use massive clusters containing a large number of heavy atoms. An example is Au_{400}^{4+} [7–10]. We show below that the conditions reached with such massive projectile–target systems lead to relaxation via new pathways as evidenced in surprising ion chemistry.

We report here the first observation of Au-adducts produced with single impacts of massive Au_n clusters, i.e. the formation and release of ejecta made from projectile atoms and target components. The experiments involved Au_n^{q+} clusters ($100 \leq n \leq 400$, $q = 4$, $34q$ keV total energy) impacting on various organic substrates, i.e. glycine, histidine and guanine. Given the constraint of a single impact in the static mode bombardment, the projectile strikes an unperturbed area of the target meaning that the formation of adducts must involve atoms from the projectile. Such a prompt in situ formation has not been predicted theoretically, nor has it been observed in MD simulations for clusters within this impact energy range. A recent MD simulation shows the formation of possible chemical bonds between carbon and silicon atoms following the impact of C_{60}^+ (250 eV/atom of impact energy) on a silicon target [11]. Ejection of the newly formed species is however not mentioned.

* Corresponding author. Tel.: +1 979 845 2341; fax: +1 979 845 1655.
E-mail address: schweikert@mail.chem.tamu.edu (E.A. Schweikert).

1387-3806/$ – see front matter © 2007 Elsevier B.V. All rights reserved.
doi:10.1016/j.ijms.2007.03.011

In the projectile–target combinations studied, the emission of Au-containing adducts is surprisingly high, with about one adduct detected per three projectile impacts. The chemistry involved must be ultra-fast (<0.1 ns) and occur under transient high pressure and temperature conditions. The newly observed production of Au-adducts is described below as a function of the parameters involved in their formation, i.e. the number of gold atoms in the projectile and the nature of the target, and compared to the yields of those for the customary secondary ions emitted from the organic solids.

2. Experimental

Targets of similar chemical properties, i.e. $1.6 < pK_{a1} < 2.34$, $9.2 < pKa2 < 9.8$, glycine ($C_2H_5NO_2$, $M_w = 75.07$), histidine ($C_6H_9N_3O_2$, $M_w = 155.16$) and guanine ($C_5H_5N_5O$, $M_w = 151.13$) were bombarded with large gold clusters, Au_n^{4+} of mean size $n = 100$, 200, 300 and 400. The targets were identically prepared by vapor deposition of analyte (film thickness ~1 μm) onto a stainless steel plate. This method of preparation assures the substrate uniformity over a large area (1 cm^2). Projectiles were impacting the targets with a total energy of 136 keV.

The experiments were run on a setup comprised of a liquid metal ion source (LMIS), a Wien filter for primary ion mass selection, a pulsed beam for single projectile bombardment and a linear time-of-flight mass spectrometer [9,12]. The LMIS used in this study, including the extraction electrode and two focusing lenses, is a duplicate of the one described by Bouneau et al. [13]. Clusters were extracted at 25 kV of acceleration potential. The primary cluster ions of interest were n/q selected through a Wien filter followed by subsequent analysis by time-of-flight. A second refined selection of the time-of-flight peak with an electronic gate allowed for the elimination of noise and fragments. However, the projectiles selected for $n/q > 9$ were always within a distribution of Au_n^{q+} clusters of various charges, q, and sizes, n, with mean values deduced from the data reported by Bouneau et al. [13].

The negative secondary ions of 9 keV energy were detected with a dual micro-channel plate (MCP) assembly with 8-anodes. Thus, the detector has the capability of recording, simultaneously, up to eight ions of the same m/z, provided they strike separate anodes. Cross-talk among anodes was determined to be <0.1% [12]. All events were collected and stored as a "Total Matrix of Events" (TME), described elsewhere [12].

3. Results

3.1. Mass spectra

We present in Fig. 1(a) the mass spectrum of negative ions emitted from a guanine target from a summation of $N_0 \sim 2 \times 10^5$ individual impacts of 136 keV Au_{400}^{4+} projectiles. The area exposed to bombardment was ~1 mm^2. Thus, the bombardment occurred under "super-static" conditions, i.e. each Au_{400}^{+} impacted a fresh area of the target. The peaks observed in the low mass range of the spectrum correspond to "conventional" secondary ions e.g., CN^-, CNO^-, C_3N^-, and larger fragments

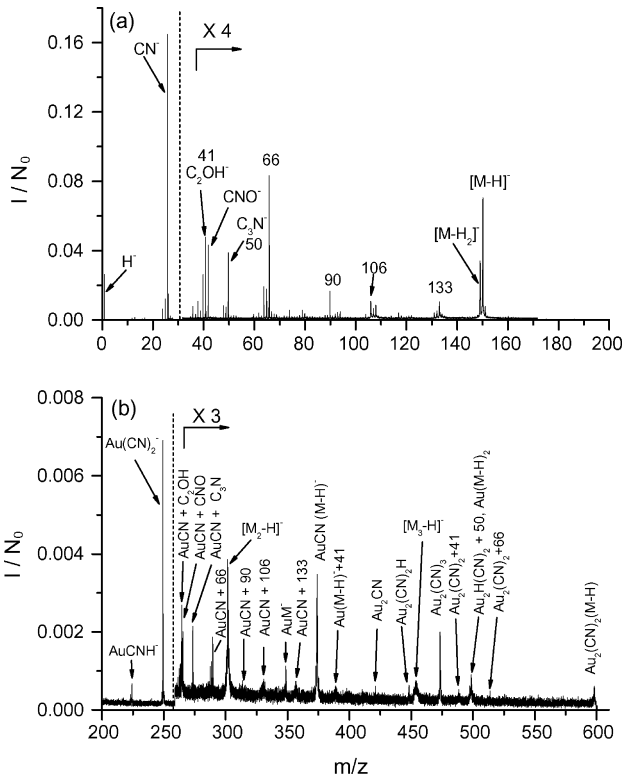

Fig. 1. (a and b) Negative mass spectra obtained from the summation of $N_0 \sim 2 \times 10^5$ individual impacts of 136 keV Au_{400}^{4+} projectiles on a guanine target. The area exposed to bombardment was ~1 mm^2.

($m/z = 66$, 90, 106 and 133) as well as the deprotonated molecular ion of guanine $(M–H)^-$. The peaks observed in the 200–600 mass range (Fig. 1(b)) are attributed to secondary ions resulting from the combination of Au and Au_2 from the incident projectile, with fragments and/or molecules from the impacted target. The variety of adducts is remarkable. $Au(CN)_2^-$ and AuCN $(M–H)^-$ are particularly notable for their abundance. The Au-adducts observed can be classified in two categories: AuX^- with X = HCN, M (molecular ion) and H and $AuCNY^-$ with Y = CN, CNO, M–H and molecular fragments (e.g. $m/z = 50$, 66, 90, 106 and 133). Au^- alone was not observed in the case of guanine.

The other series of adducts involving Au_2 is evident in Fig. 1(b). These adducts are in lower abundance but tend to be of more complex composition, combining up to three SIs from guanine versus two in the case of the Au-adducts. The prevailing Au_2-adduct is $Au_2(CN)_2X^-$ where X = CN, M–H or a molecular fragment of $m/z = 50$. Similar classes of Au and Au_2-adducts with the same respective trends in intensities were also observed in the cases of histidine and glycine.

3.2. Secondary ion yields

The quantitative abundance of the adducts can be measured with the SI yield, i.e. the number of a given SI detected per impact. The errors associated with the yield values reported below range from 0.7 to 15% for yield values ranging from 0.1 to 0.001. The experimental reproducibility was better than 10%. In Fig. 2(a and b), we show the yields for AuX^- where

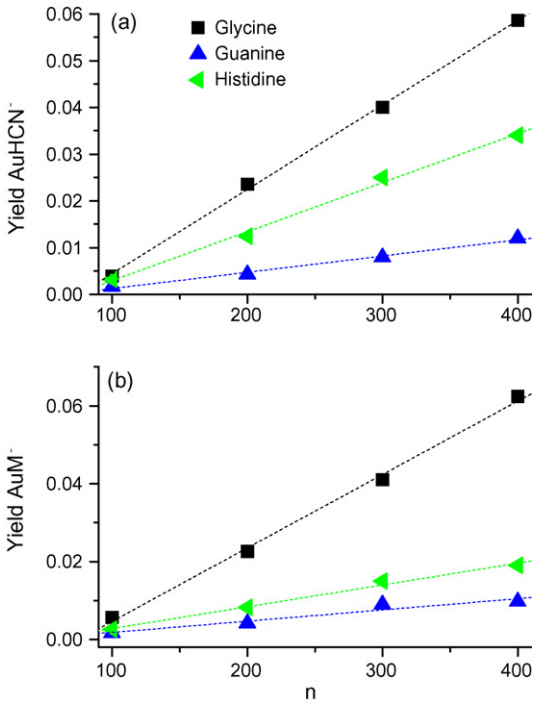

Fig. 2. Yields for the Au-adducts of type AuX^- with X = HCN (a) and X = M (b). The yields are shown for three targets (glycine, histidine and guanine) as a function of the size of the Au_n^{q+} projectile (n = 100, 200, 300, 400; q = 4). The total impact energy was 136 keV.

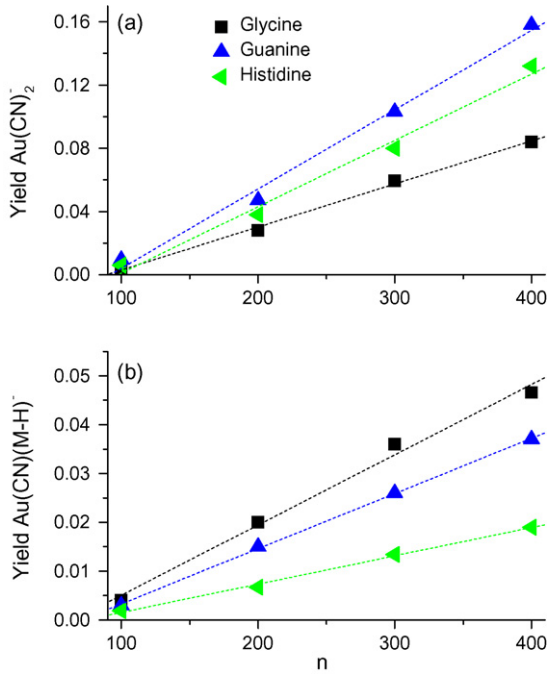

Fig. 3. Yields for the Au-adducts of type $AuCNX^-$ with X = CN (a) and X = M–H (b). The yields are shown for three targets (glycine, histidine and guanine) as a function of the size of the Au_n^{q+} projectile (n = 100, 200, 300, 400; q = 4). The total impact energy was 136 keV.

X = HCN or M as a function of the projectile size n. The yields increase linearly with the increasing number of Au atoms in the projectile for both species and the three targets. The yields for $AuHCN^-$ and AuM^- are maximum over the entire range of n for glycine and minimum for guanine. In the case of histidine, the yield for $AuHCN^-$ falls in-between those for guanine and glycine, while for AuM^- the rate of production is close to that for guanine.

The yields for more complex adducts resulting from the combination of two organic compounds with Au are presented in Fig. 3(a and b). Again, the yields increase linearly with n for the targets studied. The highest yield for $Au(CN)_2^-$ is obtained with the guanine target in a reversal of the trend for the yields for the two-body assemblies (Fig. 2). This yield reaches a maximum of 0.16 with the Au_{400}^+ projectile. For guanine, $Au(CN)_2^-$ represents half of the total production of the complex secondary ions emitted. The case for AuCN $(M–H)^-$ differs from that of $Au(CN)_2^-$ in that the yields are maximum for glycine and minimum for histidine. The trends for AuCN $(M–H)^-$ do not resemble those for the two-body assemblies (Fig. 2) since in the latter case the lowest yields were obtained for guanine. The production of AuCN $(M–H)^-$ species is smaller than that for $Au(CN)_2^-$, i.e. the maximum yield in the former case does not exceed 0.05 with the Au_{400}^+ projectile.

The occurrence of adducts can be compared with the emission of the "conventional" SIs CN^- and $(M–H)^-$. Their yields, presented in Table 1, follow trends similar to those observed with the adducts. For example, guanine generates the highest yields of CN^- and $Au(CN)_2^-$. It may be recalled that the guanine molecule contains the largest number of nitrogen, i.e. five, for the production of CN^-. The correlation between the yields for CN^- and the number of CN available per target molecule is apparent in Table 1. However, while the trends are similar, the yields for the adducts do not scale with those for CN^- or $(M–H)^-$. The difference becomes apparent when considering the ratios of the yields. The data are presented in Table 2 and

Table 1
Yields for CN^- and $(M–H)^-$ produced from glycine, histidine and guanine targets under bombardment with Au_n^{q+} projectile (n = 100, 200, 300 and 400) of 136 keV total impact energy. The error bar on the yield value is 5%

	n	Glycine	Histidine	Guanine
CN^-	400	0.7	1.1	1.6
	300	0.6	1.1	1.5
	200	0.6	1	1.3
	100	0.5	0.9	1.1
$(M–H)^-$	400	1	0.6	0.5
	300	0.8	0.5	0.5
	200	0.6	0.4	0.4
	100	0.4	0.3	0.3

Table 2
Ion yields for CN^-, $Au(CN)_2^-$, $(M–H)^-$ and AuM^- produced from guanine and histidine relative to glycine

	Guanine	Histidine
CN^-	2.24	1.72
$Au(CN)_2^-$	1.95 ± 0.39	1.47 ± 0.14
$(M–H)^-$	0.45 ± 0.05	0.73 ± 0.09
AuM^-	0.21 ± 0.05	0.37 ± 0.06

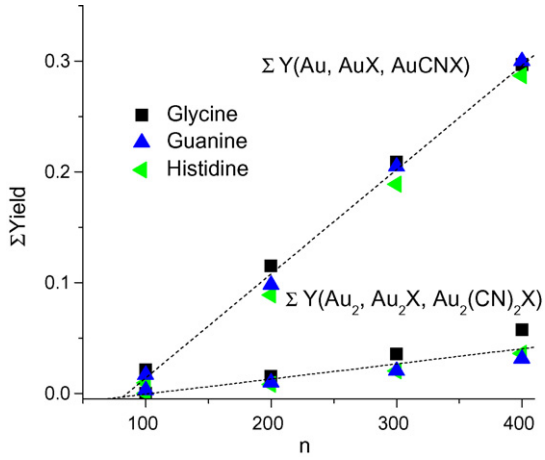

Fig. 4. Sum of the yields for Au and Au_2 containing species for three organic targets as a function of the projectile size n. The results of a fit of type $a(n-n_0)$ with $n_0 = 70$ are shown in dashed lines for Au and Au_2-adducts, respectively.

show, for example, that the yield for CN^- from guanine is 2.24 times that from glycine while the yield for $Au(CN)_2^-$ from guanine is 1.95 times that from glycine. Similar quantitative comparisons for AuM^- versus $(M–H)^-$ show that the yields for the adducts do not follow the simple relationship prevailing for the conventional SIs used as analytical signals. Further, there is no correlation between AuCN $(M–H)^-$ and $CN^-/(M–H)^-$ with respect to the nature of the molecules.

The combined yields of all the adducts containing either Au or Au_2 are presented in Fig. 4. Surprisingly, the summed yields for either class of adducts are similar for the entire set of targets although, as shown earlier (Figs. 2 and 3), the yields for specific adducts are quite different. The combined yields increase linearly with the projectile size, following a relationship of the type $a(n-n_0)$, where n_0 corresponds to the limit size of the projectile for which Au-adducts can be produced. In the present case, n_0 corresponds to 70 ± 10 atoms of gold for the targets considered.

A total yield of 0.35 for all the combined Au/Au_2-adducts is obtained with Au_{400}^{4+}. Thus, on average, one SI containing a gold atom is produced as an ionized species for every three impacts. The Au-adducts are about 7 times more abundant than those containing Au_2.

The fact that the summed yields for all adducts do not depend on the nature of the molecule indicates that the abundance of gold adducts is set by the availability of Au/Au_2 atoms/residues. We infer that the number of Au/Au_2 provided by a projectile of size n for the adduct synthesis is identical for the three target molecules examined. Indeed, the organic targets referred to here have similar physical and chemical characteristics. Therefore, the "final" condition of the projectile in the target will be identical. The formation of a specific adduct depends on the characteristics of the molecules impacted as shown in Fig. 3.

The production rate for re-emitted Au indicates that most of the gold atoms available for synthesis interact with the target components, e.g. CN, M–H, HCN and large molecular fragments. For instance, in the case of Au_{400}^{4+}, the negative gold ion as a percentage of the total gold adduct emission amounts

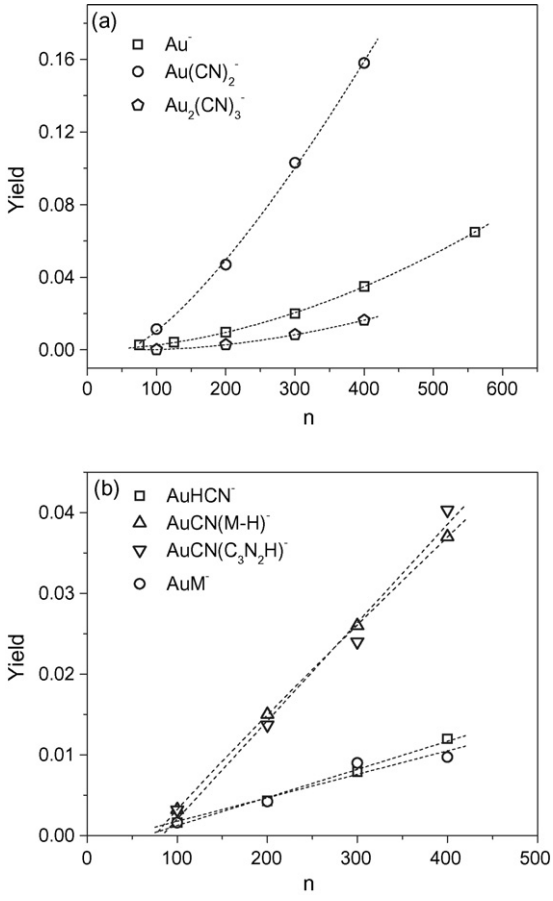

Fig. 5. Yields for Au^-, $Au(CN)_2^-$, $Au_2(CN)_3^-$ (a) and $AuHCN^-$, AuCN $(M–H)^-$, AuCN $(C_3N_2H)^-$, AuM^- (b) vs. n, size of the gold projectiles. The data are for adducts from a guanine target. The yields of re-emitted Au^- were obtained on glycine. (a) The dashed lines represent the result of a fit in n^α for Au^- ($\alpha \sim 1.8$) and a fit in $(n-n_0)^\alpha$ for $Au(CN)_2^-$ and $Au_2(CN)_3^-$ ($\alpha = 1.25$ and 1.85, respectively; $n_0 = 70$). (b) The dashed line represents the result of a fit in $(n-n_0)^\alpha$ with $\alpha = 1$ and $n_0 = 70$.

to ~10% in the bombardment of glycine, 3% in that of histidine and was not observed with guanine.

The impacted volume may be viewed as a reservoir of free radicals and molecules available for chemical reaction with Au atoms. Thus, the number of re-emitted gold ions should be correlated with the amount of molecules/free radicals available in the reservoir and the chemical affinity of the Au atoms for those compounds. The point is illustrated with guanine where the yields for CN^- and $Au(CN)_2^-$ are highest concurrently with the absence of re-emitted Au^-.

4. Discussion

4.1. Phenomenological approach

A closer examination of the yield dependence with the projectile size n for the various classes of adducts reveals some differences. The yields for $Au(CN)_2^-$ and $Au_2(CN)_3^-$ from guanine are plotted in Fig. 5(a) along with the yield for the re-emitted Au^- from glycine. As noted earlier, Au^- is not present in the mass spectra for guanine. The yield for Au^- follows a fit

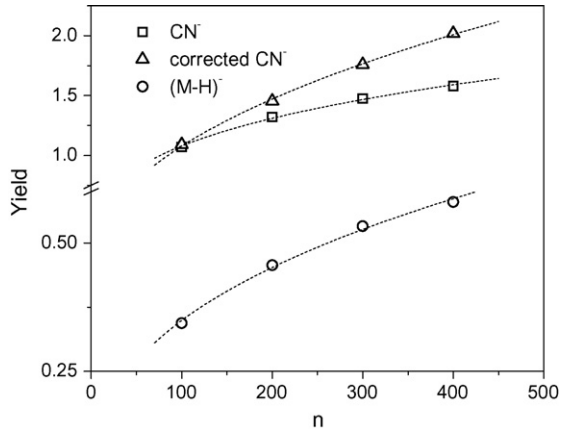

Fig. 6. Yields for CN^- and $(M–H)^-$ produced from a guanine target under bombardment with a series of Au_n^{q+} projectiles ($n = 100$, 200, 300 and 400). The value for the corrected CN^- was calculated as the sum of the yield for CN^- and all Au-adducts containing the CN fragment. The dashed line represents the result of a fit in n^α with $\alpha < 0.5$.

in n^α, with $\alpha \sim 1.8$. For $Au(CN)_2^-$ and $Au_2(CN)_3^-$, a fit with a function of the type $(n - n_0)^\alpha$ prevails. The values obtained for α were 1.24 and 1.85, respectively. The value for n_0, i.e. the minimum number of gold atoms required for adduct production, is 70 ± 10 for both $Au(CN)_2^-$ and $Au_2(CN)_3^-$.

The case for adducts of the type $AuHCN^-$, AuM^-, AuCN $(M–H)^-$ and $AuCNY^-$ is different from that of Au-adducts containing only CN. The respective yields for those species are shown in Fig. 5(b) for guanine. A fit of the data with the preceding function, i.e. $(n - n_0)^\alpha$, results in $\alpha \approx 1$. Similar relationships also prevail in the case of histidine and glycine for the two categories of adducts just described, i.e. $\alpha > 1$ for $Au(CN)_2^-$ and $Au_2(CN)_3^-$ and $\alpha \approx 1$ for Au-adducts of the type $AuHCN^-$, AuM^-, AuCN $(M–H)^-$ and $AuCNY^-$. Again, as for guanine, the values of α for the $Au_2(CN)_3^-$ ion from histidine and glycine are higher than those for $Au(CN)_2^-$. Remarkably, the value of 70 ± 10 obtained for n_0 is valid for all Au-adducts and targets considered.

The dependence of the adduct yields with projectile size must be compared with the corresponding data for conventional SIs. The yields for CN^- and $(M–H)^-$ from guanine are shown in Fig. 6. The data follow a relationship in n^α with values for α of 0.27 and 0.45 for CN^- and $(M–H)^-$, respectively. The deficit in the value of α for CN^- when compared to $(M–H)^-$ can be explained by the amount of CN involved in the adduct synthesis. Indeed, the "sequestration" of CN into gold-adducts, calculated as the sum of the yields of all Au-adducts containing CN, amounts, to ~25% of the total CN^- production in the case of guanine bombarded by Au_{400}^{4+}. The corrected yield for CN^- which takes into account the CN^- involved in the Au-adduct synthesis is shown in Fig. 6. A fit of these data as a function of n^α results in a value of 0.45 for α. A similar procedure was also applied for $(M–H)^-$. In this case, the value for α is 0.62 when the $(M–H)^-$ yield is corrected with that of the Au-adduct containing (M–H). Similar trends for the yield dependence with the size of the projectiles were also obtained for CN^- and $(M–H)^-$ produced from glycine and histidine. The values for α were systematically smaller for CN^- than that for $(M–H)^-$. This trend remains after correction for the CN and M–H present in the Au-adducts.

To summarize, the trends of the yield with the projectile size, for both classes of Au-adducts differ from those for conventional SIs. The dependence with n is more important in the case of the adducts. This is not surprising since atoms from the projectile are involved in the adduct synthesis. The difference in the value for α for various classes of Au-adducts is however surprising and suggests different pathways for the formation of $Au(CN)_2^-$ versus those of more complex composition, i.e. AuM^-, AuCN $(M–H)^-$ and AuCN combined with a molecular fragment.

4.2. Adduct formation

As noted already, two key parameters involved in the formation of adducts are the number of Au atoms available for their synthesis and the affinity of the gold atoms for the molecules or free radicals located in their vicinity. The number of Au atoms available for the adduct formation is related to the fate of the projectile in the target. The interaction of Au_{400}^{4+} with a graphite target has been examined for energies of 100 eV/atom [14,15]. High resolution transmission electron microscopy (HR-TEM) and electron diffraction show that the Au_{400}^{4+} projectiles are implanted intact as nanoparticles [15]. This observation is in agreement with an MD simulation which depicts the formation of a crater with the Au_{400}^{4+} projectile implanted "intact" at its bottom. It appears that the same condition prevails in low Z targets at a bombarding energy of 340 eV/atom. A comparison of sticky tapes irradiated with Au_{400}^{4+} at 100 and 340 eV/atom shows in both cases a pink color. Given that Au_{400}^{4+} projectiles at 100 eV/atom are implanted virtually intact in graphite, we attribute the color to gold particles with 2 nm diameter [15]. Thus, the adduct synthesis involves a small number of Au atoms evaporating in the projectile–target interaction process. This implies extensive ionization of the Au atoms detached from the projectile.

The abundance of three-body assemblies, e.g. $Au(CN)_2^-$, Au(CN) $(M–H)^-$, $Au(M_2–H)^-$ indicates a high probability of multiple interactions and consequently suggests that the adduct synthesis occurs in a dense phase. The likely existence of a dense phase is supported by the MD simulation and the experimental observation mentioned above. Indeed both studies show that the graphite in the direct vicinity of the projectile is amorphized, meaning that the material was subjected to a high energy density. If we extrapolate this observation to organic targets, the CN fragments might be produced in the crater walls. They might also be the preferred location for the formation of adducts like $Au(CN)_2^-$ or $AuCN^-$ as precursor for the formation of more complex secondary ions, since in this area Au and CN can be close enough for attractive interaction. A subsequent step leading to the formation of $AuCNX^-$ ions may occur during the expansion phase of the condensed material, i.e. during the release of the newly synthesized species outside of the crater.

Further, this dense medium may favor the survival of metastable complex ions via the dissipation of their internal

energy through a high density of neighbors. This mode of stabilization of metastable species has been documented in hot atom chemistry and may explain the survival of Au-molecular adducts [16].

5. Conclusions

A key finding is that the combined yields of the adducts are the same for different targets. We infer that the ejected matter contains an overall constant ionic charge. A further item of note is the threshold for adduct production which occurs at $n \sim 70$ under the conditions of this study.

The prompt in situ formation of Au-adducts is prolific and involves highly efficient interactions with the Au ablated from the projectile. It must be noted that the adduct emission does not scale with the abundance of the corresponding conventional SIs. Considering the conventional SIs, the CN^- and $(M–H)^-$ signals must be corrected for the amount present in the adducts in bombardment with projectile of size $n \geq 100$.

The steps leading to the re-emission of projectile atoms and residues and the production of adducts remain to be elucidated. The latter are the result of chemistry under extreme conditions. This study may be of interest due to possible similarities with astrochemical processes occurring with interstellar nano-sized dust particles that have velocities comparable to the Au projectiles used in this study.

Acknowledgements

We thank Stanislas Verkhoturov for fruitful discussions. E.A.S thanks the Robert A. Welch Foundation (A-1482) and the National Science Foundation (CHE-0449312) for funding this research. S.D.N. thanks the CNRS “direction des relations européennes et internationales” (CNRS-Etats-Unis 2006) for funding a collaborative project.

References

[1] A.D. Appelhans, J.E. Delmore, Anal. Chem. 61 (1989) 1087.
[2] M. Benguerba, A. Brunelle, S. Della Negra, J. Depauw, H. Joret, Y. Le Beyec, M.G. Blain, E.A. Schweikert, G. Ben Assayag, P. Sudraud, Nucl. Instrum. Meth. B 62 (1991) 8.
[3] G. Nagy, A.V. Walker, Int. J. Mass Spectrom. 262 (2007) 144.
[4] K. Boussofiane-Baudin, G. Bolbach, A. Brunelle, S. Della-Negra, P. Hakansson, Y. Le Beyec, Nucl. Instrum. Meth. B 88 (1994) 160.
[5] M.F. Russo Jr., I.A. Wojciechowski, B.J. Garrison, Appl. Surf. Sci. 252 (2006) 6423.
[6] E.J. Smiley, N. Winograd, B.J. Garrison, Anal. Chem. 79 (2007) 494.
[7] A. Tempez, J.A. Schultz, S. Della-Negra, J. Depauw, D. Jacquet, A. Novikov, Y. Le Beyec, M. Pautrat, M. Caroff, M. Ugarov, H. Bensaoula, M. Gonin, K. Fuhrer, A. Woods, Rapid Commun. Mass Spectrom. 18 (2004) 371.
[8] A. Novikov, M. Caroff, S. Della-Negra, J. Depauw, M. Fallavier, Y. Le Beyec, M. Pautrat, J.A. Schultz, A. Tempez, A.S. Woods, Rapid Commun. Mass Spectrom. 19 (2005) 1851.
[9] R.D. Rickman, S.V. Verkhoturov, G.J. Hager, E.A. Schweikert, Int. J. Mass Spectrom. 245 (2005) 48.
[10] C. Guillermier, S. Della Negra, R.D. Rickman, V. Pinnick, E.A. Schweikert, Appl. Surf. Sci. 252 (2006) 6529.
[11] K.D. Krantzman, D.B. Kingsbury, B.J. Garrison, Nucl. Instrum. Meth. B 255 (2007) 238.
[12] R.D. Rickman, S.V. Verkhoturov, G.J. Hager, E.A. Schweikert, J.A. Bennett, Int. J. Mass Spectrom. 241 (2005) 57.
[13] S. Bouneau, S. Della-Negra, J. Depauw, D. Jacquet, Y. Le Beyec, J.P. Mouffron, A. Novikov, M. Pautrat, Nucl. Instrum. Meth. B 225 (2004) 579.
[14] C. Anders, H.M. Urbassek, Nucl. Instrum. Meth. B 228 (2005) 57.
[15] C. Guillermier, S. Della Negra, A. Dunlop, G. Rizza, E.A. Schweikert, in preparation.
[16] K. Roessler, H.J. Jung, B. Nebeling, Adv. Space Res. 4 (1984) 83.